

Channel Estimation for Extremely Large-Scale Massive MIMO: Far-Field, Near-Field, or Hybrid-Field?

Xiuhong Wei and Linglong Dai

Abstract—Extremely large-scale massive MIMO (XL-MIMO) is a promising technique for future 6G communications. The sharp increase of BS antennas leads to the unaffordable channel estimation overhead. Existing low-overhead channel estimation schemes are based on the far-field or near-field channel model. However, the far-field or near-field channel model mismatches the practical XL-MIMO channel feature, where some scatters are in the far-field region while others may locate in the near-field region, i.e., hybrid-field channel. Thus, existing far-field and near-field channel estimation schemes cannot be directly used to accurately estimate the hybrid-field XL-MIMO channel. To solve this problem, we propose an efficient hybrid-field channel estimation scheme by accurately modeling the XL-MIMO channel. Specifically, we firstly reveal the hybrid-field channel feature of the XL-MIMO channel. Then, we propose a hybrid-field channel model to capture this feature, which contains both the far-field and near-field path components. Finally, we propose a hybrid-field channel estimation scheme, where the far-field and near-field path components are respectively estimated. Simulation results show the proposed scheme performs better than existing schemes.

Index Terms—Extremely large-scale massive MIMO, hybrid-field channel modeling, channel estimation.

I. INTRODUCTION

With the emergence of new applications, such as holographic video, digital twin, and extended reality, 6G is expected to achieve a 10-fold increase in spectrum efficiency than 5G [1]. The extremely large-scale massive MIMO (XL-MIMO) is a promising technique for 6G to achieve this goal, where the base station (BS) deploys an extremely large number of antennas to achieve higher spectral efficiency and improved energy efficiency [2]. However, the sharp increase of BS antennas leads to the unaffordable pilot overhead for the high-dimensional XL-MIMO channel estimation.

There are two typical categories of low-overhead channel estimation schemes for XL-MIMO, i.e., far-field channel estimation [3]–[5] and near-field channel estimation [6], [7]. The first category is the *far-field* channel estimation by considering the channel sparsity in the *angle domain*. In this category of schemes, the XL-MIMO channel is modeled in the far-field region with the planar wave assumption. Based on this

assumption, the array steering vector of the channel is only related to the angle. With the help of the classical discrete fourier transform (DFT) matrix, the non-sparse spatial channel can be firstly represented by the sparse angle-domain channel. Then, some compressive sensing (CS) algorithms such as orthogonal matching pursuit (OMP) [3] can be used to estimate this sparse angle-domain channel with low pilot overhead.

The second category is the *near-field* channel estimation by considering the channel sparsity in the *polar domain*. Specifically, since the antenna array aperture of XL-MIMO is very large, the XL-MIMO channel can be more accurately modeled in the near-field region with the spherical wave assumption [6], [7]. Under this assumption, the array steering vector of the channel is not only related to the angle, but also related to the distance between the BS and the scatter. Based on this near-field channel model, a new polar-domain sparse representation of the original XL-MIMO channel in the spatial domain was proposed in [6], where the transform matrix was generated from the joint angle and distance space to replace the classical DFT matrix only associated with the angle space. By considering this channel sparsity in the polar domain, the corresponding CS algorithms have been proposed to reduce the pilot overhead for the near-field channel estimation [6].

In the existing far-field or near-field channel model, it is assumed that all scatters are either in the far-field or near-field region. Actually, a hybrid-field communication environment is more likely to appear in the XL-MIMO system, where some scatters are in the far-field region, while others may locate in the near-field region. In other words, the XL-MIMO channel is usually composed of both the far-field and near-field path components. However, the existing far-field or near-field channel model mismatches this hybrid-field channel feature, which makes the existing far-field or near-field channel estimation schemes cannot be directly used to accurately estimate the hybrid-field XL-MIMO channel. Unfortunately, this important problem has not been studied in the literature.

To full in this gap, we propose an efficient hybrid-field channel estimation scheme by accurately modeling the hybrid-field XL-MIMO channel in this paper¹. Our contributions are summarized as follows.

- 1) We reveal the hybrid-field feature of the XL-MIMO channel. Specifically, this hybrid-field channel feature

All authors are with the Beijing National Research Center for Information Science and Technology (BNRist) as well as the Department of Electronic Engineering, Tsinghua University, Beijing 100084, China (e-mails: weixh19@mails.tsinghua.edu.cn, daill@tsinghua.edu.cn).

This work was supported in part by the National Key Research and Development Program of China (Grant No. 2020YFB1807201) and in part by the National Natural Science Foundation of China (Grant No. 62031019).

¹Simulation codes will be provided in the following link to reproduce the results presented in this paper after publication: <http://oa.ee.tsinghua.edu.cn/dailinglong/publications/publications.html>.

means that different scatters may be in different regions in the XL-MIMO system. On the one hand, some scatters are far away from the BS, which are in the far-field region. On the other hand, some scatters are relatively close to the BS, which are in the near-field region.

- 2) In order to capture this hybrid-field channel feature, we propose a hybrid-field channel model for the XL-MIMO channel. In the proposed hybrid-field channel model, both the far-field and near-field path components in the far-field and near-field regions are considered, which correspond to different sparse representations based on different channel transform matrices. Moreover, we can control the proportion of the two types of path components by using an adjustable parameter. In this way, the existing far-field and near-field channel models can be regarded as special cases of the proposed hybrid-field channel model.
- 3) Based on this hybrid-field channel model, we propose a hybrid-field channel estimation scheme to estimate the XL-MIMO channel with low pilot overhead. The basic idea is to individually estimate the far-field and near-field path components by using different channel transform matrices. The far-field path components are estimated by considering their sparsity in the angle domain, while the near-field path components are estimated by considering their sparsity in the polar domain. Particularly, the existing far-field and near-field channel estimation schemes can be regarded as special cases of the proposed scheme.

The rest of the paper is organized as follows. In Section II, we introduce the signal model, and review two existing channel models in the far-field and near-field. In Section III, we firstly reveal the hybrid-field channel feature, and then propose the hybrid-field channel model and the corresponding hybrid-field channel estimation scheme. Simulation results and conclusions are provided in Section IV and Section V, respectively.

Notation: Lower-case and upper-case boldface letters \mathbf{a} and \mathbf{A} denote a vector and a matrix, respectively; \mathbf{a}^H and \mathbf{A}^H denote the conjugate transpose of vector \mathbf{a} and matrix \mathbf{A} , respectively; $\|\mathbf{a}\|_2$ denotes the l_2 norm of vector \mathbf{a} . Finally, $\mathcal{CN}(\mu, \sigma)$ denotes the probability density function of the circularly symmetric complex Gaussian distribution with mean μ and variance σ^2 .

II. SYSTEM MODEL

In this section, we will first introduce the signal model of the XL-MIMO system. Then, the existing far-field and near-field channel models will be briefly reviewed, respectively.

A. Signal Model

We consider that the BS employ a N -element extremely large-scale antenna array to communicate with a single-antenna user. Let $\mathbf{h}^H \in \mathbb{C}^{1 \times N}$ denote the channel from the BS to the user. Take the downlink channel estimation as an example, the BS is required to send pilots to the user in M time slots, and then the user estimates the downlink channel

based on the received pilots. The corresponding signal model can be represented by

$$\mathbf{y}^H = \mathbf{h}^H \mathbf{P}^H + \mathbf{n}^H, \quad (1)$$

where $\mathbf{y}^H \in \mathbb{C}^{1 \times M}$ represents the received pilots by the user in M time slots, $\mathbf{P}^H \in \mathbb{C}^{N \times M}$ represents the transmitted pilot signals by the BS in M times slots, and $\mathbf{n}^H \sim \mathcal{CN}(0, \sigma^2 \mathbf{I}_M)$ represents the $M \times 1$ received noise in M times slots with σ^2 representing the noise power.

Through the conjugate transpose transformation, (1) can be further formulated as

$$\mathbf{y} = \mathbf{P} \mathbf{h} + \mathbf{n}. \quad (2)$$

The downlink channel estimation is to estimate \mathbf{h} on the premise that \mathbf{y} and \mathbf{P} are known. In the XL-MIMO system, the number of antennas N at the BS is large. In order to reduce the pilot overhead, the low-overhead channel estimation should be investigated so that the number of pilots M is much smaller than N . Next, we will briefly review two existing channel models for existing channel estimation schemes.

B. Channel Models

Specifically, as shown in Fig. 1, the electromagnetic radiation field in wireless communication systems can be divided into far-field and near-field [6], where different fields will result in different channel models. The bound between these two fields is the Rayleigh distance $Z = \frac{2D^2}{\lambda}$, where D and λ are the array aperture and wavelength, respectively.

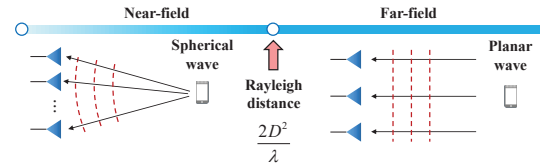


Fig. 1. The near-field region and the far-field region [6].

1) *Far-Field Channel Model:* As shown in Fig. 1, when the distance between the BS and the scatter is larger than the Rayleigh distance, the far-field channel $\mathbf{h}_{\text{far-field}}$ is modeled under the planar wave assumption, which can be represented by

$$\mathbf{h}_{\text{far-field}} = \sqrt{\frac{N}{L}} \sum_{l=1}^L \alpha_l \mathbf{a}(\theta_l), \quad (3)$$

where L represents the number of path components (corresponding to effective scatters) between the BS and the user, α_l and θ_l represent the complex gain and angle for the l th path, respectively. $\mathbf{a}(\theta_l)$ represents the far-field array steering vector based on the planar wave assumption, which can be represented by

$$\mathbf{a}(\theta) = \frac{1}{\sqrt{N}} [1, e^{-j\pi\theta}, \dots, e^{-j(N-1)\pi\theta}]^H. \quad (4)$$

In order to reduce the pilot overhead for the channel estimation, the above non-sparse channel $\mathbf{h}_{\text{far-field}}$ can be

represented by the sparse angle-domain channel $\tilde{\mathbf{h}}_{\text{Far-field}}$ with the DFT matrix \mathbf{F} as follows

$$\mathbf{h}_{\text{far-field}} = \mathbf{F}\tilde{\mathbf{h}}_{\text{far-field}}, \quad (5)$$

where $\mathbf{F} = [\mathbf{a}(\theta_1), \dots, \mathbf{a}(\theta_N)]$ is a $N \times N$ unitary matrix, where the columns are orthogonal to each other, and $\theta_n = \frac{2n-N-1}{N}$ with $n = 1, 2, \dots, N$. Since there are limited scatters in communication environments, the angle-domain channel $\tilde{\mathbf{h}}_{\text{far-field}}$ is usually sparse. Based on this sparsity, some CS algorithms can be used to estimate this high-dimensional channel with low pilot overhead [3]–[5].

2) *Near-Field Channel Model*: In addition to the above far-field channel model, a near-field channel model was recently proposed in [6]. As shown in Fig. 1, when the distance between the BS and the scatter is smaller than the Rayleigh distance, the near-field channel is modeled under the spherical wave assumption, which can be represented by

$$\mathbf{h}_{\text{near-field}} = \sqrt{\frac{N}{L}} \sum_{l=1}^L \alpha_l \mathbf{b}(\theta_l, r_l). \quad (6)$$

Compared with the far-field channel model (3), the array steering vector $\mathbf{b}(\theta_l, r_l)$ for the near-field channel model is derived based on the spherical wave assumption, which can be represented by [6]

$$\mathbf{b}(\theta_l, r_l) = \frac{1}{\sqrt{N}} [e^{-j\frac{2\pi}{\lambda}(r_l^{(1)} - r_l)}, \dots, e^{-j\frac{2\pi}{\lambda}(r_l^{(N)} - r_l)}]^H, \quad (7)$$

where r_l represents the distance from the l th scatter to the center of the antenna array, $r_l^{(n)} = \sqrt{r_l^2 + \delta_n^2 - 2r_l\delta_n d\theta_l}$ represents the distance from the l th scatter to the n th BS antenna, where $d = \frac{\lambda}{2}$ is the antenna spacing and $\delta_n = \frac{2n-N-1}{2}$, $n = 1, 2, \dots, N$.

Since the DFT matrix in (5) associated with the angle domain only matches the array steering vector in the far-field, the near-field channel (6) will cause serious energy spread in angle domain. In order to explore the sparsity of the near-field channel, [6] proposed a polar-domain transform matrix \mathbf{W} , which can be represented by

$$\mathbf{W} = [\mathbf{b}(\theta_1, r_1^1), \dots, \mathbf{b}(\theta_1, r_1^{S_1^1}), \dots, \mathbf{b}(\theta_{S_1}, r_{S_1}^1), \dots, \mathbf{b}(\theta_{S_1}, r_{S_1}^{S_1^1})], \quad (8)$$

where each column of \mathbf{W} is a near-field array steering vector with the sampled angle θ_{s_1} and distance $r_{s_1}^{s_2}$ with $s_1 = 1, 2, \dots, S_1$ and $s_2 = 1, 2, \dots, S_2^{S_1}$. Based on this polar-domain transform matrix \mathbf{W} , the near-field channel can be represented by

$$\mathbf{h}_{\text{near-field}} = \mathbf{W}\bar{\mathbf{h}}_{\text{near-field}}, \quad (9)$$

where $\bar{\mathbf{h}}_{\text{near-field}}$ is the $S \times 1$ polar-domain channel with $S = \sum_{s=1}^{S_1} S_2^s$. Similar to the far-field channel in the angle domain, $\bar{\mathbf{h}}_{\text{near-field}}$ also shows a certain sparsity. The corresponding polar-domain based CS algorithm was further proposed to reduce the pilot overhead for the near-field channel estimation [6]. However, since the polar transform matrix \mathbf{W} is generated from the joint angle and distance space, its

dimension is large, and the columns orthogonality is relatively poor compared with the classical DFT matrix. Thus, the far-field channel in the polar domain may cause more serious energy leakage than that in the angle domain.

In all existing works above, all scatters in the communication environment are assumed to be either in the far-field or near-field region. In practical XL-MIMO communication environments, it is more likely that some scatters are in the far-field region, while others may locate in the near-field region. However, this hybrid-field communication environment cannot be accurately modeled by the existing far-field or near-field channel model, so existing far-field and near-field channel estimation schemes cannot be directly used to accurately estimate the hybrid-field XL-MIMO channel.

III. PROPOSED HYBRID-FIELD CHANNEL ESTIMATION

In this section, we will firstly reveal the hybrid-field feature for the XL-MIMO channel. Then, a hybrid-field channel model will be proposed to capture this channel feature. Finally, based on the proposed channel model, we will propose a hybrid-field channel estimation scheme to improve the estimation accuracy with low pilot overhead.

A. Hybrid-Field Channel Feature

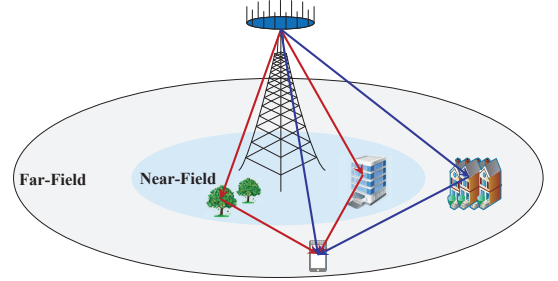


Fig. 2. The hybrid-field communication environment for XL-MIMO.

As shown in Fig. 2, there are two different types of scatters for the XL-MIMO system. When the scatter is far away from the BS, it is in the far-field region of the BS, which will introduce the far-field path component. When the scatter is close to the BS, it is in the near-field of the BS, which will produce the near-field path component. For example, when a high-altitude BS serves a distant user, although the direct link produces a far-field path component, the scatters around the BS may generate the near-field path components [6].

However, the existing far-field or near-field channel model is only composed of far-field or near-field path components, which cannot capture this hybrid-field feature of the XL-MIMO channel.

B. Proposed Hybrid-Field Channel Model

In order to capture this hybrid-field feature of the XL-MIMO channel mentioned above, we propose a hybrid-field channel model represented as

$$\mathbf{h}_{\text{hybrid-field}} = \sqrt{\frac{N}{L_f + L_n}} \left(\sum_{l_f=1}^{L_f} \alpha_{l_f} \mathbf{a}(\theta_{l_f}) + \sum_{l_n=1}^{L_n} \alpha_{l_n} \mathbf{b}(\theta_{l_n}, r_{l_n}) \right), \quad (10)$$

where L_f represents the number of far-field path components, and L_n represents the number of near-field path components. Let $\gamma = \frac{L_f}{L_f + L_n}$ denote the proportion of the far-field path components. When $\gamma = 1$, the proposed hybrid-field channel model is simplified as the existing far-field channel model. When $\gamma = 0$, the hybrid-field channel model becomes a near-field channel model. Therefore, the proposed hybrid-field channel model is a more general channel model, where the existing far-field and near-field channel models can be regarded as its special cases.

In order to estimate the hybrid-field XL-MIMO channel with low pilot overhead, we should firstly explore its sparse representation. As mentioned in Section II, the near-field path components will cause serious energy spread in the angle domain, while the far-field path components will cause serious energy leakage in the polar domain. Thus, for the hybrid-field channel consisting of both the far-field and near-field path components, the entire channel is not sparse enough neither in the angle domain nor in the polar domain. Consequently, the existing far-field and near-field channel estimation schemes cannot be directly used to accurately estimate the hybrid-field XL-MIMO channel.

C. Proposed Hybrid-Field Channel Estimation

Based on the existing OMP algorithm for far-field channel estimation, we propose a hybrid-field OMP (HF-OMP) based hybrid-field channel estimation scheme by considering the developed hybrid-field channel model. The basic idea is that, the far-field and near-field path components are respectively estimated based on different channel transform matrices. Specifically, based on (5) and (9), the channel estimation problem in (2) can be further represented as:

$$\begin{aligned} \mathbf{y} &= \mathbf{P}\mathbf{h}_f + \mathbf{P}\mathbf{h}_n + \mathbf{n} \\ &= \mathbf{P}\mathbf{F}\tilde{\mathbf{h}}_f + \mathbf{P}\mathbf{W}\bar{\mathbf{h}}_n + \mathbf{n}, \end{aligned} \quad (11)$$

where \mathbf{h}_f and \mathbf{h}_n represent the far-field path components and the near-field path components of the XL-MIMO channel $\mathbf{h}_{\text{hybrid-field}}$, respectively. $\tilde{\mathbf{h}}_f$ represents the far-field path components in the angle domain, while $\bar{\mathbf{h}}_n$ represents the near-field path components in the polar domain, which are both sparse. Therefore, if $\tilde{\mathbf{h}}_f$ and $\bar{\mathbf{h}}_n$ can be individually estimated with the reduced pilot overhead, the whole estimated channel can be directly obtained. The specific algorithm composed of three stages can be summarized in **Algorithm 1**.

The three stages of **Algorithm 1** can be explained as follows. In the first stage, the far-field path components will be estimated in the angle domain. As shown in Step 1, the far-field sensing matrix can be represented as $\mathbf{A}_f = \mathbf{P}\mathbf{F}$. Then L_f iterations will be performed to find L_f supports associated with L_f far-field path components in the angle domain. For each iteration l_f , the correlation between the sensing matrix \mathbf{A}_f and the residual vector \mathbf{r} needs to be calculated, where the most correlative column index in \mathbf{A}_f with \mathbf{r} is regarded as the newly found far-field support n^* , as shown in Step 3. Based on the updated far-field support Ω_f in Step 4, the currently estimated far-field sparse vector $\hat{\mathbf{h}}_f$ is obtained by using the least square (LS) algorithm in Step 6. After that, the residual

Algorithm 1: HF-OMP based hybrid-field channel estimation

Inputs: \mathbf{y} , \mathbf{P} , \mathbf{F} , \mathbf{W} , L_f , L_n .
Initialization: $\Omega_{\text{ff}} = \Omega_n = \emptyset$, $\mathbf{r} = \mathbf{y}$.
 // Estimate far-field path components in angle domain.
 1. $\mathbf{A}_f = \mathbf{P}\mathbf{F}$
 2. **for** $l_f = 1, 2, \dots, L_f$ **do**
 3. $n^* = \underset{n=1,2,\dots,N}{\operatorname{argmax}} \|\mathbf{A}_f^H(:, n)\mathbf{r}\|_2^2$
 4. $\Omega_f = \Omega_n \cup n^*$
 5. $\hat{\mathbf{h}}_f = \mathbf{0}_{N \times 1}$
 6. $\hat{\mathbf{h}}_f(\Omega_f) = \mathbf{A}_f^\dagger(:, \Omega_f)\mathbf{y}$
 7. $\mathbf{r} = \mathbf{y} - \mathbf{A}_f\hat{\mathbf{h}}_f$
 8. **end for**
 // Estimate near-field path components in polar domain.
 9. $\mathbf{A}_n = \mathbf{P}\mathbf{W}$
 10. **for** $l_n = 1, 2, \dots, L_n$ **do**
 11. $n^* = \underset{n=1,2,\dots,N}{\operatorname{argmax}} \|\mathbf{A}_n^H(:, n)\mathbf{r}\|_2^2$
 12. $\Omega_n = \Omega_{\text{nf}} \cup n^*$
 13. $\hat{\mathbf{h}}_n = \mathbf{0}_{S \times 1}$
 14. $\hat{\mathbf{h}}_n(\Omega_n) = \mathbf{A}_n^\dagger(:, \Omega_n)\mathbf{y}$
 15. **if** $\Omega_f \neq \emptyset$ **then**
 16. $\mathbf{r} = \mathbf{y} - \mathbf{A}_n\hat{\mathbf{h}}_n - \mathbf{A}_f\hat{\mathbf{h}}_f$
 17. **else**
 18. $\mathbf{r} = \mathbf{y} - \mathbf{A}_n\hat{\mathbf{h}}_n$
 19. **end**
 20. **end for**
 // Obtain all path components.
 21. $\hat{\mathbf{h}} = \mathbf{0}_{N \times 1}$
 22. **if** $\Omega_f \neq \emptyset$ **then**
 23. $\hat{\mathbf{h}} = \hat{\mathbf{h}} + \mathbf{F}\hat{\mathbf{h}}_f$
 24. **if** $\Omega_n \neq \emptyset$ **then**
 25. $\hat{\mathbf{h}} = \hat{\mathbf{h}} + \mathbf{W}\hat{\mathbf{h}}_n$
 26. **end**
Output: Estimated hybrid-field channel $\hat{\mathbf{h}}$.

vector \mathbf{r} is updated by removing the contribution of far-field path components that have been estimated. Finally, we can obtain the finally estimated far-field path components $\hat{\mathbf{h}}_f$ in the angle domain after L_f iterations.

In the second stage, the near-field path components will be estimated in the polar domain with the near-field sensing matrix $\mathbf{A}_n = \mathbf{P}\mathbf{W}$. The process of this stage is similar to that of the first stage, with only two differences. The first difference is that, the near-field sparse vector $\hat{\mathbf{h}}_n$ to be estimated in Step 14 is an $S \times 1$ vector, whose dimension is generally much higher than that of the far-field sparse vector $\hat{\mathbf{h}}_f$. The second difference is that, when updating the residual vector \mathbf{r} , not only the contribution of the estimated near-field path components but also that of all estimated far-field path components (if there exist) should be removed.

After estimating the far-field path components in the angle domain and the near-field path components in the polar domain, we can obtain the entire estimated channel $\hat{\mathbf{h}}$ on the

basis of (5) and (9), as shown in Steps 21-26. It is noted that both the existing far-field OMP and near-field OMP algorithms can be regarded as special cases of the proposed HF-OMP algorithm by respectively setting $L_n = 0$ (i.e., $\gamma = 1$) and setting $L_f = 0$ (i.e., $\gamma = 0$).

Finally, the computational complexity of the proposed HF-OMP algorithm is analyzed as follows. Since the calculation steps in the first stage and the second stage of **Algorithm 1** are similar to those in the existing OMP algorithm, the computational complexity of the first stage and the second stage can be directly obtained as the $\mathcal{O}(NML_f^3)$ and $\mathcal{O}(SML_n^3)$ by referring to the OMP algorithm [4]. In the third stage, the computational complexity mainly comes from Step 23 and Step 25, which can be represented by $\mathcal{O}(NS)$. To sum up, the overall computational complexity of the proposed HS-OMP algorithm is $\mathcal{O}(NML_f^3) + \mathcal{O}(SML_n^3) + \mathcal{O}(NS)$.

IV. SIMULATION RESULTS

For simulations, we consider the number of BS antennas $N = 512$ and the number of pilots $M = 256$. Each element of the pilot matrix \mathbf{P} is randomly selected from $\{-\frac{1}{\sqrt{M}}, +\frac{1}{\sqrt{M}}\}$. The wavelength is set as $\lambda = 0.01$ meters, corresponding to the 30 GHz frequency. The near-field path components are generated in the distance range of [10, 100] meters. The number of the sampled grids for the polar-domain transform matrix \mathbf{W} is set to $S = 2071$, which is generated according to the method described in [6]. The SNR is defined as $1/\sigma^2$.

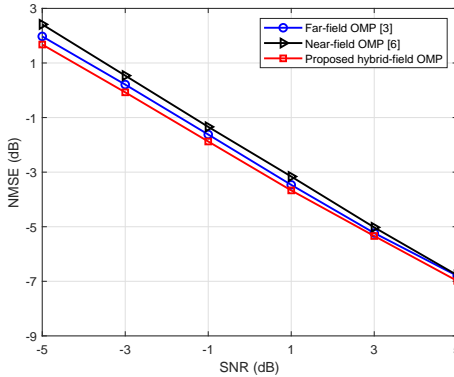


Fig. 3. NMSE performance comparison against the SNR by considering the hybrid-field channel model.

We compare the proposed HF-OMP based hybrid-field channel estimation scheme with the existing far-field OMP based scheme [3] and the near-field OMP based scheme [6]. It is noted that since the transform matrices are generated on the sampled grids, the number of non-zero elements is larger than the number of paths. Thus, in the considered three schemes, $8L_f + 8L_n$ non-zero elements should be estimated.

Fig. 3 shows the normalized mean square error (NMSE) performance comparison against the SNR, where the numbers of far-field and near-field path components are $L_f = 3$ and $L_n = 3$, respectively. we can find that, the proposed HF-OMP based scheme can achieve better NMSE performance than existing far-field based OMP scheme and the near-field based OMP scheme.

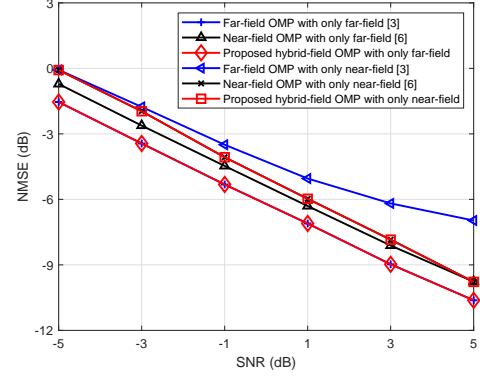


Fig. 4. NMSE performance comparison against the SNR by only considering far-field or near-field channel model.

Fig. 4 provides the NMSE performance comparison when only the far-field path components ($L_f = 3$ and $L_n = 0$) or only the near-field path components ($L_f = 0$ and $L_n = 3$) are considered. We can find that the proposed HF-OMP based scheme always achieves the best performance out of all three considered schemes. Particularly, we can also verify that the far-field OMP based scheme and the near-field OMP based scheme can be regarded as special cases of the proposed HF-OMP based scheme.

V. CONCLUSIONS

In this paper, we have proposed a hybrid-field channel estimation scheme by accurately modeling the hybrid-field XL-MIMO channel. It is shown that the existing far-field and near-field channel estimation schemes can be regarded as special cases of the proposed hybrid-field channel estimation scheme. Simulation results show that the proposed scheme can achieve better NMSE performance with the same low pilot overhead. For future works, more advanced CS algorithms can be used to solve the hybrid-field channel estimation problem with improved performance.

REFERENCES

- [1] M. Giordani, M. Polese, M. Mezzavilla, S. Rangan, and M. Zorzi, "Toward 6G networks: Use cases and technologies," *IEEE Commun.Mag.*, vol. 58, no. 3, pp. 55–61, Mar. 2020.
- [2] E. D. Carvalho, A. Ali, A. Amiri, M. Angelichinoski, and R. W. Heath, "Non-stationarities in extra-large-scale massive MIMO," *IEEE Wireless Commun.*, vol. 27, no. 4, pp. 74–80, Aug. 2020.
- [3] J. Lee, G. Gil, and Y. H. Lee, "Channel estimation via orthogonal matching pursuit for hybrid MIMO systems in millimeter wave communications," *IEEE Trans. Wireless Commun.*, vol. 64, no. 6, pp. 2370–2386, Jun. 2016.
- [4] X. Gao, L. Dai, S. Zhou, A. M. Sayeed, and L. Hanzo, "Wideband beamspace channel estimation for millimeter-wave MIMO systems relying on lens antenna arrays," *IEEE Trans. Signal Process.*, vol. 67, no. 18, pp. 4809–4824, Sep. 2019.
- [5] X. Wei, C. Hu, and L. Dai, "Deep learning for beamspace channel estimation in millimeter-wave massive MIMO systems," *IEEE Trans. Commun.*, vol. 69, no. 1, pp. 182–193, Jan. 2021.
- [6] M. Cui and L. Dai, "Channel estimation for extremely large-scale MIMO: Far-field or near-field?" *arXiv preprint arXiv:2108.07581*, Aug. 2021.
- [7] X. Yin, S. Wang, N. Zhang, and B. Ai, "Scatterer localization using large-scale antenna arrays based on a spherical wave-front parametric model," *IEEE Trans. Wireless Commun.*, vol. 16, no. 10, pp. 6543–6556, Jul. 2017.